Structure, Physical, and Photophysical Properties of Platinum(II) Complexes Containing Bidentate Aromatic and Bis(diphenylphosphino)methane as Ligands

J. DePriest,[†] G. Y. Zheng,[‡] N. Goswami,[‡] D. M. Eichhorn,*[,‡] C. Woods,[†] and D. P. Rillema*[,‡]

Department of Chemistry, Wichita State University, Wichita, Kansas 67260-0051, and Department of Chemistry, The University of Tennessee, Knoxville, Tennessee 37996

Received November 8, 1999

This study focuses on a series of $Pt^{II}(L-L')(dppm)^{n+}$ complexes, where dppm is bis(diphenylphosphino)methane and L−L′ are C^C′ ($n = 0$), C^N ($n = 1$), and N^N′ ($n = 2$) aromatic ligands. Structural characteristics are as follows: for $[Pt(phen)(dppm)](PF_6)_2$, a N^N′ derivative, monoclinic, $C2/c$, $a = 33.583(6)$ Å, $b = 11.399(2)$ Å, $c = 22.158(4)$ Å, $Z = 8$; for $[Pt(phq)(dppm)](PF_6)$, a C^N derivative, triclinic, $P\bar{1}$, $a = 11.415(3)$ Å, $b = 13.450(3)$ Å, $c = 14.210(4)$ Å, $Z = 2$; for $[Pt(phpy)(dppm)](PF_6)$, a C^N derivative, triclinic, $P\bar{1}$, $a = 10.030(3)$ Å, $b = 13.010(2)$ Å, $c = 15.066(4)$ Å, $Z = 2$; and for [Pt(bph)(dppm)], a C^C′ derivative, $P2_1/c$, $a = 17.116(7)$ Å, $b = 21.422(6)$ Å, $c = 26.528(6)$ Å, $Z = 12$, where phen is 1,10-phenanthroline, phq is 2-phenylquinoline, phpy is 2-phenylpyridine, and bph is 2,2′-biphenyl. Structural features indicate that the Pt−C bond distance is shorter than the Pt−N bond distance in symmetrical complexes and that the Pt−P bond distance trans to N is shorter than the Pt−P bond trans to C. This is consistent with the ^{31}P NMR spectra where the chemical shift of the P trans to C is ∼10 ppm less than found for P trans to N. The energy maxima of the metal-to-ligand charge-transfer band for the complexes containing various L−L′ ligands occur in the near-UV region of the spectrum and fall into the energy series bpy > bph > phen > 2-phpy > 2-ptpy > 2-phq > 7,8-bzq, where bpy is 2,2′-bipyridine, 2-phpy is 2-phenylpyridine, 2-ptpy is 2-*p*-tolylpyridine, and 7,8-bzq is 7,8-benzoquinoline. The emission energy maxima, ascribed to variance in metal-perturbed triplet ligand centered emission, commence near 500 nm and follow the series phen > bpy > 7,8-bzq > 2-phpy > 2-ptpy > bph > 2-phq. In general, emission is observed at 77 K and in solution at low temperatures, but the temperature dependence of the emission lifetimes indicates thermal activation to another state occurs with an energy of ∼1800 cm^{-1} for the complexes, with the exception of [Pt(bph)(dppm)], which has an activation energy of ∼2300 cm^{-1}.

Introduction

Several platinum(II) complexes containing cis C^C′, C^N, and N^N′ aromatic ligands have been reported to luminesce both in solution and in the solid state.[1−50] The assigned source of the emission in solution or in the solid state where stacking does not occur has been attributed to ligand-centered emission, metal-perturbed ligand-centered emission, and metal-to-ligand

* To whom correspondence should be addressed..
[†] The University of Tennessee.
[‡] Wichita State University.

(1) Miskowski, V. M.; Houlding, V. H.; Che, C.-M.; Wang, Y. *Inorg. Chem.* **1993**, *32*, 2518.
(2) Houlding, V. H.; Miskowski, V. M. *Coord. Chem.* **1991**, *111*, 145.
(3) Miskowski, V. M.; Houlding, V. H. *Inorg. Chem.* **1991**, *30*, 4446.
(4) Miskowski, V. M.; Houlding, V. H. *Inorg. Chem.* **1989**, *28*, 1529.
(5) Craig, C. A.; Garces, F. O.; Watts, R. J.; Palmans, R.; Frank, A. J. *Coord. Chem.* **1990**, *97*, 193.
(6) Mdleleni, M. M.; Bridgewater, J. S.; Watts, R. J.; Ford, P. C. *Inorg. Chem.* **1995**, *34*, 2334.
(7) Che, C.-M.; Yam, V. W.-W.; Wong, W.-T.; Lai, T.-F. *Inorg. Chem.* **1989**, *28*, 2908.
(8) Che, C.-M.; Wan, K.-T.; He, L.-Y.; Poon, C.-K.; Yam, V. W.-W. *J. Chem. Soc., Chem. Commun.* **1989**, 943.
(9) Wan, K.-T.; Che, C.-M. *J. Chem. Soc., Chem. Commun.* **1990**, 140.
(10) Che, C.-M.; He, L.-Y.; Poon, C.-K.; Mak, T. C. W. *Inorg. Chem.* **1989**, *28*, 3081.
(11) Wan, K.-T.; Che, C.-M.; Cho, K.-C. *J. Chem. Soc., Dalton Trans.* **1991**, 1077.
(12) Chan, C.-W.; Lai, T.-F.; Che, C.-M.; Peng, S.-M. *J. Am. Chem. Soc.* **1993**, *115*, 11245.
(13) Sacksteder, L.; Baralt, E.; DeGraff, B. A.; Lukehart, C. M.; Demas, J. N. *Inorg. Chem.* **1991**, *30*, 2468.
(14) Martin, M.; Krough-Jesperson, M.-B.; Hsu, M.; Tewksbury, J.; Laurent, M.; Viswanath, K.; Patterson, H. *Inorg. Chem.* **1983**, *22*, 647 and references therein.
(15) von Zelwesky, A.; Belser, P.; Hayoz, P.; Dux, R.; Hua, X.; Suckling, A.; Stoeckli-Evans, H. *Coord. Chem. Rev.* **1994**, *132*, 75.
(16) Maestri, M.; Sandrini, D.; von Zelewsky, A.; Deuschel-Cornioley, C. *Inorg. Chem.* **1991**, *30*, 2476.
(17) Deuschel-Cornioley, C.; von Zelewsky, A. *Inorg. Chem.* **1987**, *26*, 3354.
(18) Barigelletti, F.; Sandrini, D.; Maestri, M.; Balzani, V.; von Zelewsky, A.; Chassot, L.; Jolliet, P.; Maeder, U. *Inorg. Chem.* **1988**, *27*, 3644.
(19) Maestri, M.; Sandrini, D.; Balzani, V.; von Zelewsky, A.; Deuschel-Cornioley, C.; Jolliet, P. *Helv. Chim. Acta* **1988**, *71*, 1053.
(20) Chassot, L.; von Zelewsky, A.; Sandrini, D.; Maestri, M.; Balzani, V. *J. Am. Chem. Soc.* **1986**, *108*, 6084.
(21) Maestri, M.; Sandrini, D.; Balzani, V.; Chassot, L.; Jolliet, P.; von Zelewsky, A. *Chem. Phys. Lett.* **1985**, *122*, 375.
(22) Chassot, L.; Muller, E.; von Zelewsky, A. *Inorg. Chem.* **1984**, *23*, 4249.
(23) Chassot, L.; von Zelewsky, A. *Helv. Chim. Acta* **1983**, *66*, 2443.
(24) Blanton, C. B.; Murtaza, Z.; Shaver, R. J.; Rillema, D. P. *Inorg. Chem.* **1992**, *31*, 3230.
(25) Blanton, C. B.; Rillema, D. P. *Inorg. Chim. Acta* **1990**, *168*, 145.
(26) Chen, Y. H.; Merkert, J. W.; Murtaza, Z.; Woods, C.; Rillema, D. P. *Inorg. Chim. Acta* **1995**, *240*, 41.
(27) DePriest, J.; Zheng, G. Y.; Woods, C.; Rillema, D. P.; Mikirova, N. A.; Zandler, M. E. *Inorg. Chim. Acta* **1997**, *264*, 287.
(28) Zheng, G. Y.; Rillema, D. P.; Reibenspies, J. H. *Inorg. Chem.* **1998**, *37*, 3588.
(29) Kunkely, H.; Vogler, A. *J. Am. Chem. Soc.* **1990**, *112*, 5625.
(30) Cummings, S. D.; Eisenberg, R. *J. Am. Chem. Soc.* **1996**, *118*, 1949.
(31) Cummings, S. D.; Eisenberg, R. *Inorg. Chim. Acta* **1996**, *242*, 225.
(32) Bevilacqua, J. M.; Eisenberg, R. *Inorg. Chem.* **1994**, *33*, 1886.
(33) Cummings, S. D.; Eisenberg, R. *Inorg. Chem.* **1995**, *34*, 2007.
(34) Cummings, S. D.; Eisenberg, R. *Inorg. Chem.* **1995**, *34*, 3396.
(35) Bevilacqua, J. M.; Eisenberg, R. *Inorg. Chem.* **1994**, *33*, 1886.

10.1021/ic991306d CCC: $19.00
Published on Web 04/06/2000

charge-transfer emission. However, in the solid state where the platinum centers are about 3.3 Å apart, the origin of emission is reported to occur from a metal-centered excited state or a low-lying π^* state. Systems where metal-centered emission occurred contained simple ligands such as cyanide, whereas the π^* emitters contained heterocyclic or aromatic ligands. But in general, excited-state assignments have been open to interpretation and have varied from author to author. In some earlier studies, the focus has been on specific C^C′, C^N, or N^N′ systems. Further, the ancillary ligands have often been different, making a ready comparison of physical and photophysical properties between the various complexes difficult.

In this paper the behavior of a series of platinum(II) complexes containing bidentate aromatic ligands coordinated in two adjacent sites via C^C′ donor atoms, C^N donor atoms, or N^N′ donor atoms is examined in order to evaluate properties based on systematic ligand changes. The other two coordination sites were fixed with the same ligand, bis(diphenylphosphino)-methane. Here, we examine X-ray structures of four complexes containing each ligand type, the ^{31}P NMR spectral shifts resulting from the trans influence of P trans to C or N, and the electronic and emission properties as the donor atoms are altered between carbanion and nitrogen electron pair donors.

Experimental Section

Materials. Pt(bph)(CO)$_2$,[26] [Pt(7,8-bzq)(dppm)](PF$_6$),[27] and Pt-(dppm)Cl$_2$ [51] were prepared according to previously published procedures. All solvents were HPLC grade. Methylene chloride, methanol, and toluene were optima grade, purchased from Fisher Scientific, and used as received. Absolute ethanol was purchased from McCormick Distilling Co. Ethanol and methanol were used in a 4:1 (v/v) mixture to prepare the solutions for emission studies. *N*-Butyronitrile was 98% and purchased from Aldrich. Atlantic Microlabs, Inc., Norcross, Georgia, performed elemental analyses.

Preparation of Compounds. (a) Pt(dppm)(NO$_3$)Cl. Pt(dppm)-(NO$_3$)Cl was prepared by the addition of 1 equivalent of AgNO$_3$ (0.0288 g, 0.169 mmol) in 5 mL of water to a rapidly stirred solution of Pt-(dppm)Cl$_2$ (0.1102 g, 0.169 mmol) in 200 mL of CH$_2$Cl$_2$ contained in a flask wrapped with Al foil. After 5 min, the water layer became opaque. Sufficient acetone was added (200 mL) until the solutions emulsified. After the resulting AgCl suspension was stirred for 30 min, the AgCl was separated by suction filtration and the light-yellow oil was evaporated to near dryness (water bath temperature of 80°C). The light-yellow oil was dissolved in 50 mL of CH$_2$Cl$_2$ and placed in a freezer at −15 °C for 8 h. Ice crystals were easily separated by gravity filtration. The light-yellow CH$_2$Cl$_2$ solution was reduced to 10 mL and used in situ for subsequent experiments. The product was characterized by ^{31}P{^{1}H} NMR spectroscopy.

(b) Pt(dppm)(NO$_3$)$_2$. Pt(dppm)(NO$_3$)$_2$ was prepared according to the same procedure as for Pt(dppm)(NO$_3$)Cl, employing Pt(dppm)Cl$_2$ (0.9101 g, 1.10 mmol) and 2.2 equiv of AgNO$_3$ (0.5231 g, 3.08 mmol). Isolation of this product was not attempted. However, since this compound was a precursor to others, the completeness of Pt(dppm)Cl$_2$ conversion to Pt(dppm)(NO$_3$)$_2$ was verified in each synthesis using ^{31}P-{^{1}H} NMR spectroscopy.

(c) [Pt(2-phpy)(dppm)](PF$_6$). The precursor Pt(dppm)(NO$_3$)$_2$ was prepared using Pt(dppm)Cl$_2$ (0.9104 g, 1.40 mmol) and AgNO$_3$ (0.5231 g, 3.08 mmol). The ligand 2-phenylpyridine was introduced into the light-yellow acetone/CH$_2$Cl$_2$ solution by adding 5.5 mL of a previously prepared 0.32 M solution of the ligand in CH$_2$Cl$_2$. After the solution was stirred at room temperature for 72 h, the solvent was removed using a rotary evaporator (80 °C water bath). To the residue formulated as [Pt(2-phpy)(dppm)](NO$_3$), 5.0 equiv of NH$_4$PF$_6$ (1.1410 g, 7.00 mmol) was added as a dry white solid and the mixture was dissolved in 100 mL of acetone. The mixture was stirred for 1 h and then evaporated to dryness. The light-orange solid was dried under vacuum at room temperature for 24 h.

A 55 mL barreled (1.2 cm inside diameter × 50 cm) flash chromatography column with a 250 mL solvent flask head was prepared in the following manner. Silica gel, which was oven-dried at 140 °C prior to use, was loaded onto the column and then washed with 70 mL of CH$_2$Cl$_2$ and rinsed with 70 mL of hexanes. The orange solid was loaded onto the column and stoppered with a glass wool plug. The solid was eluted using a CH$_2$Cl$_2$/hexanes (70/30, v/v) solvent mixture. Four bands appeared on the column after using 4000 mL of eluant. From the column top, band 1 was dark-brown and narrow (0−2 cm wide); band 2 was red-orange and narrow (2−6 cm wide); band 3 was yellow-green and less narrow (13−17 cm); band 4 was light-green, broad (30−50 cm), and far removed from the third band.

The fourth band contained the product [Pt(2-phpy)(dppm)]$^+$ as indicated by ^{31}P{^{1}H} NMR spectroscopy. The only peaks present were those due to the cation and the PF$_6^-$ anion. The ratio of the areas of the cation peaks to the anion peaks was 2. The product was further purified by repetitive slow crystal growth from CH$_2$Cl$_2$/ethanol and hexanes solvent mixtures. A light yellow-green solid was obtained after several recrystallizations. It was vacuum-dried. Yield: 56% (0.6835 g). Anal. Calcd for [Pt(2-phpy)(dppm)](PF$_6$): C, 49.21; H, 3.44. Found: C, 50.07; H, 3.93. Single crystals suitable for X-ray structure analysis were obtained by slow diffusion of diethyl ether into a methylene choride solution containing the complex.

(d) [Pt(2-ptpy)(dppm)]PF$_6$. [Pt(2-ptpy)(dppm)]PF$_6$ was prepared and purified according to the same procedures as that for making [Pt-(2-phpy)(dppm)](PF$_6$). The preparation consisted of using Pt(dppm)-Cl$_2$ (0.9321 g, 1.43 mmol), AgNO$_3$ (0.5356 g, 3.15 mmol), 2-(*p*-tolyl)pyridine (0.5410 g, 3.20 mmol), and NH$_4$PF$_6$ (1.3690 g, 8.40 mmol). A light yellow-green solid was obtained, which formed fibrous sheets when air-dried. Yield: 65% (0.8313 g). Anal. Calcd for [Pt(2-ptpy)(dppm)]PF$_6$: C, 49.78; H, 3.61. Found: C, 49.78; H, 3.73.

(e) [Pt(2-phq)(dppm)]PF$_6$. [Pt(2-phq)(dppm)]PF$_6$ was prepared and purified according to the same methods employed to make [Pt(2-phpy)-(dppm)](PF$_6$). The preparation procedure using Pt(dppm)Cl$_2$ (0.8980 g, 1.38 mmol), AgNO$_3$ (0.5160 g, 3.04 mmol), 2-phenylquinoline (0.5954 g, 2.90 mmol), and NH$_4$PF$_6$ (1.4221 g, 8.72 mmol) resulted in isolation of a light-yellow solid. Initially, this method gave a relatively large amount of material with an estimated 1% phosphorus-containing impurity. Efforts to remove the impurity via repeated column chromatography as described for [Pt(2-phpy)(dppm)](PF$_6$) dramatically decreased the yield. Initial yield: 68% (0.8721 g). Final yield: 37% (0.4750 g). Single crystals suitable for X-ray structure analysis were

(36) Bevilacqua, J. M.; Eisenberg, R. *Inorg. Chem.* **1994**, *33*, 2913.
(37) Bevilacque, J. M.; Zuleta, J. A.; Eisenberg, R. *Inorg. Chem*. **1993**, *32*, 3689.
(38) Zuleta, J. A.; Bevilacqua, J. M.; Proserpio, B. M.; Harvey, P. D.; Eisenberg, R. *Inorg. Chem.* **1992**, *31*, 2396.
(39) Aldridge, T. K.; Stacy, E. M.; McMillin, D. P. *Inorg. Chem.* **1994**, *33*, 722.
(40) Bailey, J. A.; Hill, M. G.; Marsh, R. E.; Miskowski, V. M.; Schaefer, W. P.; Gray, H. B. *Inorg. Chem.* **1995**, *34*, 4591.
(41) Bailey, J. A.; Miskowski, V. M.; Gray, H. B. *Inorg. Chem.* **1993,** *32*, 369.
(42) Roundhill, D. M.; Gray, H. G.; Che, C.-M. *Acc. Chem. Res*. **1989**, *22*, 55 and references therein.
(43) Schindler, J. H.; Fukuda, R. C.; Adamson, A. W. *J. Am. Chem. Soc*. **1982**, *104*, 3596.
(44) Hidvegi, I.; von Ammon, W.; Gliemann, G. *J. Chem. Phys.* **1982**, *76*, 4361.
(45) Schwarz, R.; Linder, M.; Gliemann, G. *Ber. Bunsen-Ges. Phys. Chem.* **1987**, *91*, 1233.
(46) Biedermann, J.; Wallfahrer, M.; Gliemann, G. *J. Lumin.* **1987**, *37*, 323.
(47) Schwarz, R.; Gliemann, G.; Chassot, L.; Jolliet, P.; von Zelewsky, A. *Helv. Chim. Acta* **1989**, *72*, 224.
(48) Lechner, A.; Gliemann, G. *J. Am. Chem. Soc*. **1989**, *111*, 7469 and references therein.
(49) Biedermann, J.; Gliemann, G.; Klement, U.; Range, K.-J.; Zabel, M. *Inorg. Chim. Acta* **1990**, *169*, 63.
(50) Gliemann, G.; Yersin, H. *Structure and Bonding*; Springer-Verlag: Berlin, 1985; pp 87−153.
(51) McEwan, D. M.; Pringle, P. G.; Shaw, B. L. *J. Chem. Soc., Chem. Commun.* **1982**, 1240.
(52) Demas, J. N.; Crosby, G. A. *J. Phys. Chem*. **1971**, *75*, 991.
(53) *TeXsan: Crystal Structure Analysis Package*; Molecular Structure Corporation, 1985 and 1992.

obtained by slow diffusion of diethyl ether into a methylene choride solution containing the complex.

(f) [Pt(bpy)(dppm)](PF$_6$)$_2$. [Pt(bpy)(dppm)](PF$_6$)$_2$ was prepared according to a method similar to that used to make [Pt(2-phpy)(dppm)](PF$_6$). The preparative procedure using Pt(dppm)Cl$_2$ (0.6697 g, 1.03 mmol), AgNO$_3$ (0.4317 g, 2.54 mmol), 2,2′-bipyridine (0.3527 g, 2.26 mmol), and NH$_4$PF$_6$ (1.5902 g, 9.76 mmol) resulted in the isolation of a white solid. [Pt(bpy)(dppm)](PF$_6$)$_2$ decomposed upon exposure to silica gel in both CH$_2$Cl$_2$ and acetone solutions. Hence, purification was achieved by stripping the crude reaction mixture containing excess NH$_4$PF$_6$ to dryness and extracting the product with 3 × 30 mL portions of CH$_2$Cl$_2$. (NH$_4$PF$_6$ is insoluble in CH$_2$Cl$_2$.) The CH$_2$Cl$_2$ extracts were combined and reduced to 30 mL. Then 100 mL of ethanol and 30 mL of hexanes were added, and the resulting solution was allowed to stand undisturbed (several hours) until small colorless crystals emerged. Several successive crops of crystals were obtained, and each crop was evaluated for purity by ^{31}P{^{1}H} NMR. (The ratio of the area of the peak for [Pt(bpy)(dppm)]$^{2+}$ to that of PF$_6^-$ must equal 1:1.) Finally, the product was recrystallized from acetone by adding anhydrous diethyl ether until precipitation was complete. The product, a white solid, was dried in vacuo. Yield: 24% (0.2548 g). Anal. Calcd for [Pt(bpy)(dppm)](PF$_6$)$_2$: C, 40.99; H, 2.95. Found: C, 40.76; H, 2.96.

(g) [Pt(phen)(dppm)](PF$_6$)$_2$. [Pt(phen)(dppm)](PF$_6$)$_2$ was synthesized according to the same method used to make [Pt(bpy)(dppm)](PF$_6$)$_2$. The reagents used were Pt(dppm)Cl$_2$ (0.6558 g, 1.01 mmol), AgNO$_3$ (0.3752 g, 2.21 mmol), 1,10-phenanthroline (0.3528 g, 1.96 mmol), and NH$_4$PF$_6$ (1.8036 g, 11.06 mmol). The light-green solid obtained was more resistant to decomposition than [Pt(bpy)(dppm)](PF$_6$)$_2$ under the stated conditions. Purification was achieved by employing the methods used for [Pt(bpy)(dppm)](PF$_6$)$_2$. Yield: 77% (0.8145 g). Anal. Calcd for [Pt(phen)(dppm)](PF$_6$)$_2$: C, 42.34; H, 2.88. Found: C, 42.42; H, 2.96. Single crystals for X-ray diffraction studies were obtained from the recrystallization matrix described for purification of [Pt(bpy)(dppm)](PF$_6$)$_2$.

(h) [Pt(bph)(dppm)]·$^1/_3$CH$_2$Cl$_2$. A 50 mL flask was charged with 40 mg (1 × 10^{-4} mol) of Pt(bph)(CO)$_2$ powder and 10 mL of methylene chloride. Then 38 mg (1 × 10^{-4} mol) of dppm (bis(diphenylphosphino)-methane) was added to the Pt(bph)(CO)$_2$ suspension. The solution immediately turned bright-yellow, and gas bubbles evolved. The reaction mixture was stirred overnight. The resulting yellow solution was then filtered with a fine-fritted funnel, and the solvent was removed with a rotary evaporator. The yellow solid remaining in the flask was then dissolved in a minimum amount of methylene chloride, and hexane was added dropwise until the solution turned cloudy. The cloudy solution was placed in the freezer overnight, and the yellow precipitate that formed was collected in a fine-fritted funnel by suction filtration. The yellow solid was washed with hexane and dried under vacuum. The solid retained approximately $^1/_3$ mole of CH$_2$Cl$_2$ per mole of complex, even after repeated evacuations. The yield was 65 mg (89%). ^{1}H NMR (CDCl$_3$): δ 7.8−7.7(m, 8H), 7.5−7.3(m, 16H), 6.9(t, 18 Hz, 2H), 6.6(t, 18 Hz, 2H), 5.3 (s, 0.71H), 2.4−2.1(m, 4H). Anal. Calcd for [Pt(bph)(dppm)]·$^1/_3$CH$_2$Cl$_2$: C, 58.99; H, 4.03; Cl, 3.12. Found: C, 58.63; H, 4.16; Cl, 3.45. Single crystals suitable for X-ray structure analysis were obtained by slow diffusion of diethyl ether into a methylene choride solution of the complex.

Physical Measurements. UV−visible spectra were recorded with a Olis Cary 14 spectrophotometer equipped with a photomultiplier tube (PMT). The UV−vis absorption spectra were measured at room temperature in CH$_2$Cl$_2$.

NMR spectra were obtained with a JEOL FX90Q Fourier transform NMR spectrometer. ^{31}P{^{1}H} spectra were recorded at 36.21 MHz using 85% H$_3$PO$_4$ as the external reference. The instrument was locked on the deuterium signal of acetone-d_6.

Emission spectra were recorded with a Spex Fluorolog 212 spectrofluorometer equipped with a double monochromator and PMT as the detector. All emission spectra were measured in a mixture of C$_2$H$_5$OH/CH$_3$OH in 4:1 (v/v) at either room temperature or 77 K and corrected for instrument response. Samples were degassed by more than three freeze−pump−thaw cycles prior to measurement. For the quantum yield measurement, rhodamine B base (ϕ_r = 0.71)[52] was used as a standard, and the equation

$$\phi_s = \phi_r \frac{A_r}{A_s}\frac{I_s}{I_r} \quad (1)$$

was used to calculate the emission quantum yields. ϕ_s is the quantum yield of the sample, ϕ_r is the quantum yield of reference rhodamine B, A_s and A_r are the absorbance of the sample and the reference at 355 nm, respectively, and I_s and I_r are integrated areas under the emission spectra.

Excited-state lifetimes were measured by exciting the samples at 355 nm with an OPOTEK optical parametric oscillator pumped by a frequency-tripled Nd:YAG laser (Continuum Surlite, run at <1.5 mJ/10 ns pulse). Spectra regions were isolated with a Hamamatsu R955 PMT in a cooled housing (−15 °C, Amherst) coupled to an Acton SpectraPro 275 monochromator. Transients were recorded with a LeCroy 9359A digital oscilloscope (1 Gs/s). Oscilloscope control and data curve fitting were accomplished with a program developed in house. Variable temperature emission lifetimes from 90 to 270 K were measured by adding a Cryo Industries EVT cryostat controlled by a Lakeshore 805 temperature controller to the above system. The cryostat was modified in house by adding a larger copper thermal mass, then calibrating with an auxiliary thermocouple using ice−water as the reference junction. This resulted in a temperature accuracy of ±1.6 K over the 90−270 K range. For temperatures above 270 K, the samples were equilibrated outside the Dewer by a Fisher Isotemp bath with the thermostated water circulating between the sample holder and the water bath.

The temperature-dependent lifetimes were then fit to

$$\tau^{-1} = \tau_0^{-1} + k_1\, e^{-\Delta E/(RT)} \quad (2)$$

where τ_0 is the lifetime at 0 K, k_1 is the preexponential constant, ΔE is the activation energy for the excited-state decay process, and R is a constant and equals 0.695 cm^{-1} K^{-1}.

X-ray Crystallography of 1−3. Crystals of **1** and **2** (**1**, yellow plates, dimensions 0.70 mm × 0.30 mm × 0.15 mm; **2**, green blocks, dimensions 0.30 mm × 0.20 mm × 0.10 mm) were affixed to a glass fiber using epoxy. The data were collected at room temperature. A crystal of **3** (yellow block, dimensions 0.15 mm × 0.10 mm × 0.10 mm) was affixed to a glass fiber using Paratone-N oil (Exxon) and transferred to the nitrogen stream of the diffractometer operating at −110 °C. Data for all three structures were collected on an Enraf-Nonius CAD4 diffractometer equipped with graphite monochromatized Mo Kα radiation (λ = 0.710 73 Å) and controlled by software running on a SGI 02 computer. Monitoring of three intense reflections every hour revealed no significant intensity fluctuations. The unit cells were determined from the setting angles of 24 reflections with 20° < 2θ < 24° and confirmed by axial photographs. For **1**, 17 902 reflections were collected (ω−2θ; +h, +k, ±l; 2° < 2θ < 50°), giving a unique set of 17 315 reflections (R_{int} = 0.094) and 9534 observed reflections (I > 2σ(I)). For **2**, 6701 reflections were collected (ω−2θ; +h, ±k, ±l; 2° < 2θ < 50°), giving a unique set of 6349 reflections (R_{int} = 0.080) and 4708 observed reflections (I > 2σ(I)). For **3**, 5393 reflections were collected (ω−2θ; +h, ±k, ±l; 2° < 2θ < 45°), giving a unique set of 5044 reflections (R_{int} = 0.032) and 4608 observed reflections (I > 2σ(I)). The data were processed and the structures solved and refined using the TeXsan package.[53] The data for **1** were corrected for secondary extinction (8.2496 × 10^{-9}). The data for **1**−**3** were corrected for Lorentz and polarization effects with an empirical absorption correction using the DIFABS[54] program (max/min transmission factors: **1**, 1.0/0.67; **2**, 1.0/0.80; **3**, 1.0/0.62). The structures were solved by direct methods[55]

(54) Walker, N.; Stuart, D. I. DIFABS. *Acta Crystallogr.* **1983**, *A39*, 158.
(55) Altomare, A.; Cascarano, M.; Giacovazzo, C.; Guagliardi, A. SIR92. *J. Appl. Crystallogr.* **1993**, *26*, 343.
(56) Creagh, G. H.; McAuley, W. J. I*nternational Tables for Crystallography*; Wilson, A. J. C., Ed.; Kluwer Academic Publishers: Boston, 1992; Vol. C.

Table 1. Crystal and Structure Refinement Data for [Pt(dppm)(bph)] (**1**), [Pt(dppm)(2-phq)](PF_6) (**2**), [Pt(dppm)(phpy)](PF_6) (**3**), and [Pt(dppm)(phen)](PF_6)$_2$ (**4**)

	1	**2**	**3**	**4**
formula	$C_{37}H_{30}P_2Pt$	$C_{40}H_{32}F_6NP_3Pt$	$C_{44}H_{50}F_6NP_3PtO_2$	$C_{37}H_{30}F_{12}N_2P_4Pt$
fw	750.02[b]	928.7	1026.86	1049.6
temp (°C)	20	20	−110	20
λ (Å)	0.710 69	0.710 69	0.710 69	0.710 69
cryst syst	monoclinic	triclinic	triclinic	monoclinic
space group	$P2_1/c$	$P\bar{1}$	$P\bar{1}$	$C2/c$
a (Å)	17.116(7)	11.415(3)	10.030(3)	33.583(6)
b (Å)	21.422(6)	13.450(3)	13.010(2)	11.399(2)
c (Å)	26.528(6)	14.210(4)	15.066(4)	22.158(4)
α (deg)	90	61.85(2)	93.20(2)	90
β (deg)	100.82(3)	73.27(2)	91.13(2)	112.60(1)
γ (deg)	90	72.70(2)	99.21(2)	90
V (Å^3)	9554(5)	1808(1)	1936.8(8)	7831(2)
Z	12	2	2	8
ρ_{calcd} (g/cm^3)	1.564	1.705	1.76	1.781
μ (cm^{-1})	45.14	40.59	38.01	38.35
R1[a]	0.045	0.044	0.037	0.047
wR2[a]	0.041	0.041	0.042	0.1267

[a] $R1 = \sum(|F_o| - |F_c|)/\sum|F_c|$ and $wR2 = ((\sum(w(F_o^2 - F_c^2)^2/\sum wF_o^4)^{1/2}$. [b] Formula weight includes $^1/_3H_2O$ and $^1/_6(C_2H_5)_2O$ per Pt complex.

Table 2. Selected Bond Distances and Angles for **1**−**4**

Bond Distance, Å							
1		**2**		**3**		**4**	
Pt(1)−P(11)	2.310(3)	Pt(1)−P(1)	2.219(2)	Pt(1)−P(1)	2.318(2)	Pt−P1	2.257(3)
Pt(1)−P(12)	2.300(3)	Pt(1)−P(2)	2.342(2)	Pt(1)−P(2)	2.228(2)	Pt−P2	2.247(3)
Pt(1)−C(101)	2.05(1)	Pt(1)−C(1)	2.047(7)	Pt(1)−C(11)	2.038(7)	Pt−N1	2.082(8)
Pt(1)−C(112)	2.05(1)	Pt(1)−N(1)	2.122(6)	Pt(1)−N(1)	2.073(6)	Pt−N2	2.074(8)
Angle, deg							
1		**2**		**3**		**4**	
C(101)−Pt(1)−C(112)	80.9(4)	C(1)−Pt(1)−N(1)	79.2(3)	C(11)−Pt(1)−N(1)	79.7(3)	N1−Pt−N2	79.0(3)
P(11)−C(125)−P(12)	95.2(5)	P(1)−C(28)−P(2)	94.8(4)	P(1)−C(24)−P(2)	95.2(4)	P1−C1−P2	91.7(5)
P(11)−Pt(1)−P(12)	73.10(9)	P(1)−Pt(1)−P(2)	72.99(8)	P(1)−Pt(1)−P(2)	73.33(7)	P1−Pt−P2	71.39(10)

and refined by full-matrix least-squares techniques with values for Δf and $\Delta f'$ from Creagh and McAuley.[56]

In the structure of **1**, the asymmetric unit contained three molecules of the Pt complex, a molecule of water, and a $^1/_2$ occupied molecule of diethyl ether. In the structure of **3**, two disordered molecules of diethyl ether were found in the asymmetric unit, each of which was modeled by two overlapping molecules of 50% occupancy. The carbon atom bound to Pt (C11) in structure **3** could not be modeled with anisotropic thermal parameters and was thus refined isotropically. All other non-hydrogen atoms except those in the solvent molecules in **1** and **3** were refined with isotropic thermal parameters. Hydrogen atoms in the Pt complexes were included at idealized positions but were not refined. Pertinent details are given in Table 1.

X-ray Crystallography of 4. A yellow crystal of **4** (dimensions 0.60 mm × 0.25 mm × 0.20 mm) was mounted on a glass fiber with epoxy resin. Diffraction data were collected at 20 °C on a Siemens R3mV diffractometer equipped with graphite monochromatic Mo Kα radiation (λ = 0.710 73 Å). Three standard reflections were monitored for every 97 reflections collected and exhibited no significant intensity fluctuations during the data collection. Lattice constants were optimized in each case from a least-squares refinement of a group of high-angle reflections in the range $20° < 2\theta < 35°$. Corrections for Lorentz and polarization effects were made. The data collection method was ω scans. An absorption correction based on ψ scans was applied. The maximum and minimum transmission factors were 0.626 and 0.394, respectively. With the use of the library of programs in the SHEXLTL package,[57] the structure was solved by Patterson methods and subsequent Fourier difference synthesis and refined using full-matrix least-squares refinement on F_o^2. The residual R1 is the conventional R index based on F_o for $I_o > 2\sigma(I_o)$. The weighed R index based on F_o^2 is reported as wR2. During the later stages of refinement, hydrogen atoms were included at their calculated positions (d(C−H) = 0.96 Å) but were not refined. The largest residual electron densities in the difference maps were in the vicinity of a heavy metal or a disordered hexafluorophosphate group and were not deemed chemically significant. There are two hexafluorophosphate anions per cation. One anion is wholly contained within the asymmetric unit and is disordered. Modeling of the disorder led to assignment of three orientations with site occupations of approximately 0.45, 0.29, and 0.20. The second anion in the asymmetric unit is formed from two-half anions, since the two phosphorus atoms lie on special positions, each with 0.5 occupancy. Other experimental crystallographic data are listed in Table 1.

Results

Structures of Complexes. Selected bond distances and angles for **1**−**4** are listed in Table 2. Figure 1 shows drawings of the complexes. For **1**, the structure of one of the three independent molecules is shown; the other two molecules are essentially identical. The structures of **1**−**4** are approximately square planar with two sites occupied by the phosphorus atoms of the primary dppm ligand and the other two sites occupied by carbon or nitrogen donor atoms of the aromatic secondary ligand. A notable observation about the structures is that the Pt−P bonds trans to a Pt−C bond are longer than Pt−P bonds trans to a Pt−N bond. The average Pt−P bond length in **1** is 2.305 Å, and it is 2.252 Å in **4**. The Pt−P bond trans to the Pt−C bond in **2** is 2.342 Å, and it is 2.318 Å in **3**. The Pt−P bond in **2**

(57) Sheldrick, G. M. *SHELXTL/PC*, version 5; Siemens Analytical X-ray Instruments, Inc.; Madison, WI, 1995.
(58) Pregosin, P. S.; Kunz, R. W. In *^{31}P and ^{13}C NMR of Transition Metal Phosphine Complexes*; Diehl, P., Fluck, E., Kosfield, R., Eds.; Springer-Verlag: New York, 1979; Chapters 2, 3, and 6.
(59) Hassan, F. S. M.; McEwan, D. M.; Pringle, P. G.; Shaw, B. L. *J. Chem. Soc., Dalton Trans.* **1985**, 1501.

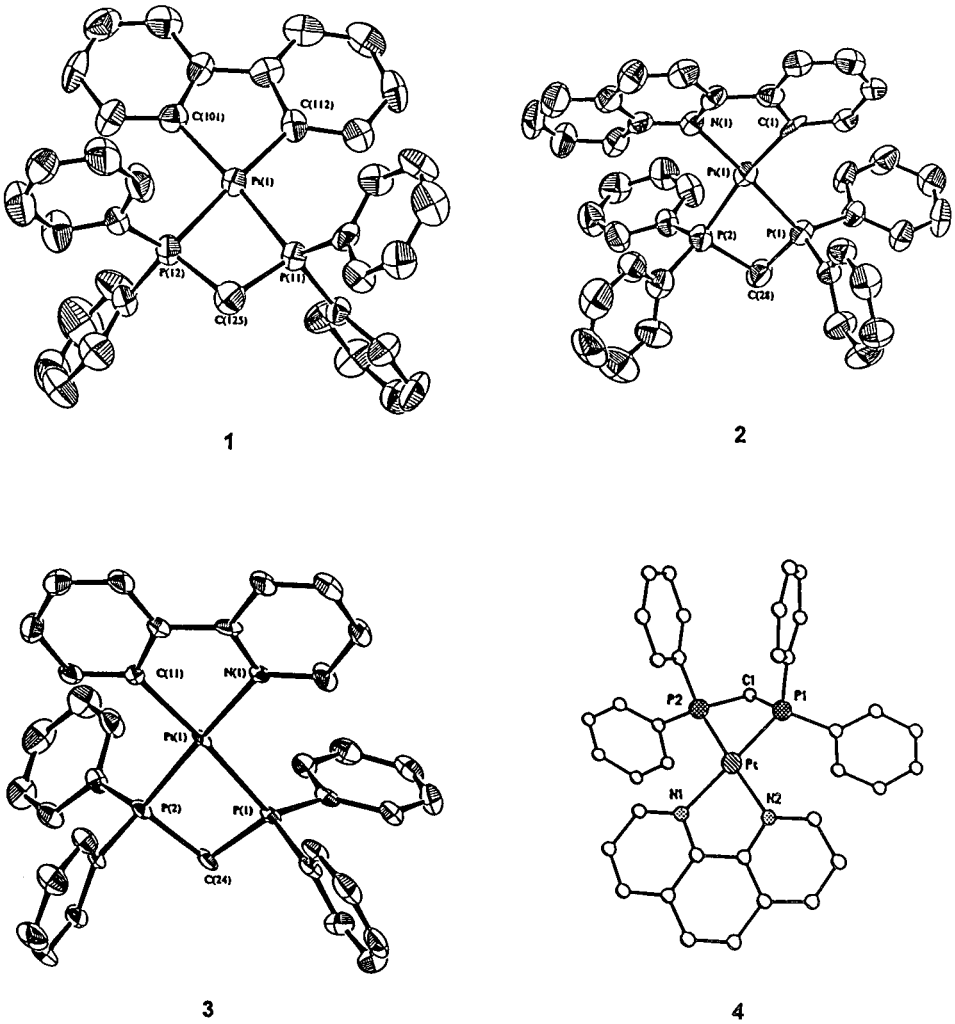

Figure 1. Plots of the structures of [Pt(bph)(dppm)] (**1**), [Pt(2-phq)(dppm)]$^+$ (**2**), [Pt(2-phpy)(dppm)]$^+$ (**3**), [Pt(phen)(dppm)]$^{2+}$ (**4**).

trans to the Pt−N bond is 2.219 Å, and it is 2.228 Å in **3.** A possible explanation for this occurrence is the greater σ donation of an anionic carbon atom over that of a neutral nitrogen atom, leading to a lengthening of the Pt−P bond trans to the carbon.

Other structural features of interest are the Pt−C and Pt−N bond lengths. In **1** and **4**, Pt−C bond distances are on average 0.05 Å shorter than Pt−N bond lengths. In **2**, a structure that is well defined, there is a 0.075 Å difference but only a 0.035 Å difference in **3**. The strucure of **3** may be disordered because of the inability to distinguish C from N crystallographically, which may account for the smaller difference. However, platinum(II) complexes do show structural variations. For example, the Pt−C and Pt−N bond distances of the related [Pt(7,8-bzq)(dppp)]$^+$ were 2.100(9) and 2.084(10) Å, respectively.

^{31}P{^{1}H} NMR Spectra. ^{31}P{^{1}H} NMR data are given in Table 3. The assignment of δ and ^1J(Pt−P) values corresponding to their trans atoms is based on reported criteria[58,59] but is also obvious by comparing data of [Pt(C^N)(dppm)]$^+$ to [Pt(C^C′)(dppm)] and [Pt(N^N′)(dppm)]$^{2+}$. The δ values for P trans to the C site ranged from −25.3 to −28.4 ppm, and the δ values for P trans to N ranged from −33.5 to −36.8 ppm for [Pt(C^N)(dppm)]$^+$ and from −52.3 to −53.1 ppm for [Pt(N^N′)(dppm)]$^{2+}$. The ^1J(Pt−P) values for P trans to C ranged from 1357 to 1572 Hz and from 2866 to 3555 Hz for P trans to N. ^nJ(P−P) coupling values were calculated for [Pt(C^N)(dppm)]$^+$ using the relationship ^nJ(P−P) = ^2J(PCP) + ^2J(PPtP), where the observed coupling constant is the sum of coupling through the ^2J(PCP) and ^2J(PPtP) paths.[60] The ^nJ(P−P) values were approximately 40 Hz.

Table 3. NMR ^{31}P{^{1}H} NMR Spectral Data

compound	X[a]	δ(Pt−P),[b] ppm	^1J(Pt−P),[c] Hz	^nJ(Pt−P),[c] Hz
Pt(dppm)Cl$_2$	Cl	−64.4	3077	
Pt(dppm)(Cl)(NO$_3$)	NO$_3$	−68.4	3233	73
	Cl	−61.4	3266	73
Pt(dppm)(NO$_3$)$_2$	NO$_3$	−69.4	3403	
[Pt(dppm)(2-phpy)]PF$_6$	C	−26.6	1406	39
	N	−34.6	3403	39
[Pt(dppm)(2-ptpy)]PF$_6$	C	−25.3	1401	39
	N	−34.0	3403	39
[Pt(dppm)(2-phq)]PF$_6$	C	−27.3	1357	44
	N	−33.5	3555	44
[Pt(dppm)(bpy)]PF$_6$	N,N′	−53.1	2817	
[Pt(dppm)(phen)]PF$_6$	N,N′	−52.3	2866	
[Pt(dppm)(7,8-bzq)]PF$_6$	C	−28.2	1445	44
	N	−36.1	3390	44
[Pt(bph)(dppm)]	C,C′	−28.4	1572	

[a] X indicates the ligand trans to phosphorus. [b] Chemical shift data, δ(Pt−P). [c] ^1J(Pt−P) and ^nJ(P−P): ±0.6 Hz.

(60) Jameson, C. J. In *Phosphorous-31 NMR Spectroscopy in Stereochemical Analysis*; Verkade, J. G., Quin, L. D., Eds.; VCH: Deerfield Beach, FL, 1987; Chapter 6, pp 215−217, 223−224.
(61) Wang, Y.; Perez, W.; Zheng, G. Y.; Rillema, D. P. *Inorg. Chem.* **1998**, *37*, 2051.

Table 4. UV−Vis Absorption Properties of Pt(II) Complexes in CH_2Cl_2

complex	λ (nm) {ϵ (10^3 cm^{-1} M^{-1})}				
[Pt(bph)(dppm)]	342 (5.46 ± 0.15)	309 (4.54 ± 0.28)	284 (23.6 ± 1.4)	255 (50.7 ± 2.8)	
$[Pt(2\text{-phpy})(dppm)]^+$	362 (2.03 ± 0.04)	332 (6.42 ± 0.09)	323 (6.18 ± 0.08)	274 (27.7 ± 1.3)	268 (29.1 ± 1.3)
$[Pt(2\text{-ptpy})(dppm)]^+$	372 (2.60 ± 0.009)	338 (6.30 ± 0.022)	326 (6.20 ± 0.03)	275 (31.5 ± 0.2)	269 (31.2 ± 0.2)
$[Pt(2\text{-phq})(dppm)]^+$	394 (3.11 ± 0.06)	355 (12.8 ± 0.1)	340 (11.5 ± 0.1)	277 (20.0 ± 2.1)	
$[Pt(7,8\text{-bzq})(dppm)]^+$	406 (2.30 ± 0.02)	386 (2.32 ± 0.02)	345 (2.33 ± 0.02)	301 (19.2 ± 0.1)	
$[Pt(bpy)(dppm)]^{2+}$	334 (7.30 ± 0.13)	320 (12.8 ± 0.23)	315 (13.1 ± 0.2)	275 (21.6 ± 0.8)	268 (24.1 ± 1.4)
$[Pt(phen)(dppm)]^{2+}$	358 (1.62 ± 0.02)	340 (2.34 ± 0.01)	285 (30.9 ± 0.1)	277 (33.5 ± 0.1)	

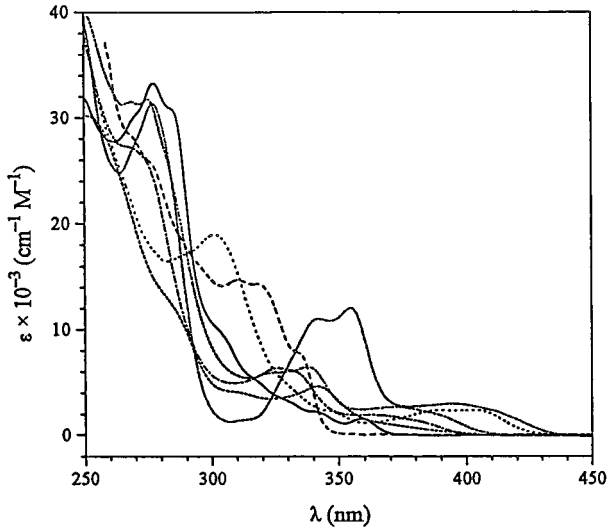

Figure 2. UV−vis absorption spectra of Pt(II) complexes in CH_2Cl_2 at 296 K: (− − −) [Pt(bph)(dppm)]; (−•−) [Pt(2-phpy)(dppm)](PF_6); (-••) [Pt(2-ptpy)(dppm)](PF_6); (-•-) [Pt(2-phq)(dppm)](PF_6); (- - -) [Pt-(7,8-bzq)(dppm)](PF_6); (— — —) [Pt(bpy)(dppm)]$(PF_6)_2$; (—) [Pt(phen)-(dppm)]$(PF_6)_2$.

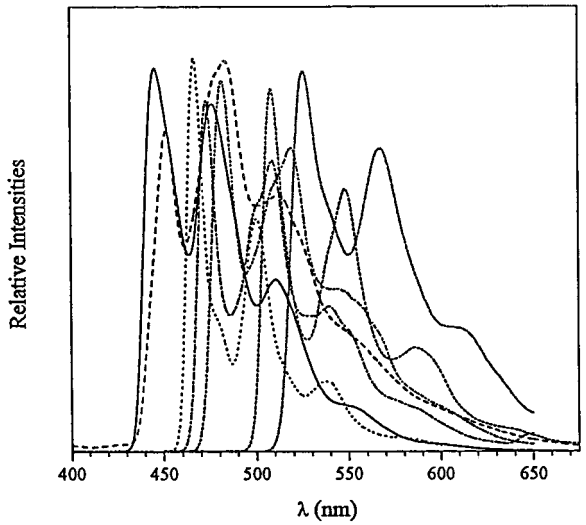

Figure 3. Emission spectra of Pt(II) complexes in 4:1 (v/v) C_2H_5OH/CH_3OH at 77 K excited at 355 nm: (− − −) [Pt(bph)(dppm)]; (−•−) [Pt(2-phpy)(dppm)](PF_6); (-••) [Pt(2-ptpy)(dppm)](PF_6); (-•-) [Pt(2-phq)-(dppm)](PF_6); (- - -) [Pt(7,8-bzq)(dppm)](PF_6); (— — —) [Pt(bpy)-(dppm)]$(PF_6)_2$; (—) [Pt(phen)(dppm)]$(PF_6)_2$.

UV−Vis Absorption Spectra. The UV−vis absorption spectra for the Pt complexes are shown in Figure 2. Absorption energy maxima and extinction coefficients for the complexes in CH_2Cl_2 are listed in Table 4. The free ligands show strong transitions in the UV region, which are assigned as $\pi\pi^*$ transitions, but no transitions were observed in the visible region. When the ligands were complexed with Pt(II), higher energy absorption features were observed and were attributed to ligand-centered $\pi\pi^*$ transitions perturbed by complexation with the Pt(II) center while new transition bands were observed at lower energy. These lower energy bands were assigned as metal-to-ligand charge transfer (MLCT) transitions on the basis of their positions, intensities, and comparison to analgous systems.[24,27,61] The MLCT transition decreased in energy as the aromatic ligand changed from bpy to bzq as follows:

$$\text{bpy} > \text{bph} > \text{phen} > \text{2-phpy} > \text{2-ptpy} > \text{2-phq} > \text{7,8-bzq} \quad (3)$$

Emission Spectra. The emission spectra were measured in 4:1 (v/v) C_2H_5OH/CH_3OH at 77 K and are compared in Figure 3. Each spectrum showed four prominent bands with vibrational progressions of 1400−1500 cm^{-1}. The emission energy maxima for the complexes are compiled in Table 5. The emission energy maximum varied from 20.8 × 10^3 cm^{-1} for $[Pt(ptpy)(dppm)]^+$ to 22.5 × 10^3 cm^{-1} for $[Pt(phen)(dppm)]^{2+}$. The series follow the trend in increasing energy order as follows:

$$\text{2-phq} < \text{bph} < \text{2-ptpy} < \text{2-phpy} < \text{7,8-bzq} < \text{bpy} < \text{phen} \quad (4)$$

Emission spectra were independent of the excitation energy; excitation at different wavelengths resulted in the same emission profiles.

Table 5. Emission Properties of Pt(II) Complexes[a]

complex	ν_{max} ± 0.05 (10^3 cm^{-1})		
[Pt(bph)(dppm)]	19.65	8.24	17.09
$[Pt(2\text{-phpy})(dppm)]^+$	20.98	19.53	18.42
$[Pt(2\text{-ptpy})(dppm)]^+$	20.62	19.19	18.18
$[Pt(2\text{-phq})(dppm)]^+$	19.01	17.61	16.31
$[Pt(7,8\text{-bzq})(dppm)]^+$	21.28	19.88	18.48
$[Pt(bpy)(dppm)]^{2+}$	21.99	20.53	19.42
$[Pt(phen)(dppm)]^{2+}$	22.17	20.75	19.38

[a] 4:1 (v/v) C_2H_5OH/CH_3OH.

Emission Lifetimes. Emission lifetimes were measured in 4:1 (v/v) C_2H_5OH/CH_3OH at 77 K and are listed Table 6. For the dppm complexes, the emission lifetimes at 77 K decreased from 1170 to 16.7 μs in the series phen (1170 μs) > 7,8-bzq (204 μs) > 2-ptpy (61 μs) > 2-phq (55 μs) > 2-phpy (47 μs) > bpy (27.1 μs) > bph (16.7 μs).

Emission lifetimes were also measured over the 80−300 K temperature range, and this temperature dependence is shown in Figure 4. At temperatures from 80 to 120 K, the lifetime decreased very slowly with an increase in temperature. At temperatures from 120 to 140 K, the glass-to-fluid transition,

(62) Barltrop, J. A.; Coyle, J. D. *Excited States in Organic Chemistry*; Wiley: New York, 1975; pp 53−61.
(63) Zheng, G. Y.; Rillema, D. P. Unpublished observations.

Table 6. Emission Lifetime Properties of Pt(II)(dppm) Complexes[a]

complex	τ_{77} (ms)	ΔE (10^3 cm^{-1})	ln k_1	τ_{296K} (ns)	$\phi_{296K} \times 10^4$
[Pt(bph)(dppm)]	16.7 ± 1.4	2.20 ± 0.07	28.2 ± 0.4	24.6	15
[Pt(2-phpy)(dppm)]$^+$	47.6 ± 0.9	1.83 ± 0.04	31.3 ± 0.3	0.19	1.7
[Pt(2-ptpy)(dppm)]$^+$	60.6 ± 2.2	1.79 ± 0.02	29.5 ± 0.1		
[Pt(2-phq)(dppm)]$^+$	54.9 ± 1.5	1.77 ± 0.06	28.0 ± 0.5	3.76	1.5
[Pt(7,8-bzq)(dppm)]$^+$	204 ± 5	1.81 ± 0.02	31.0 ± 0.2	0.23	8.8
[Pt(bpy)(dppm)]$^{2+}$	27.1 ± 1.9	1.62 ± 0.05	23.3 ± 0.3	200	5.9
[Pt(phen)(dppm)]$^{2+}$	1170 ± 60				

[a] 4:1 (v/v) C_2H_2OH/CH_3OH.

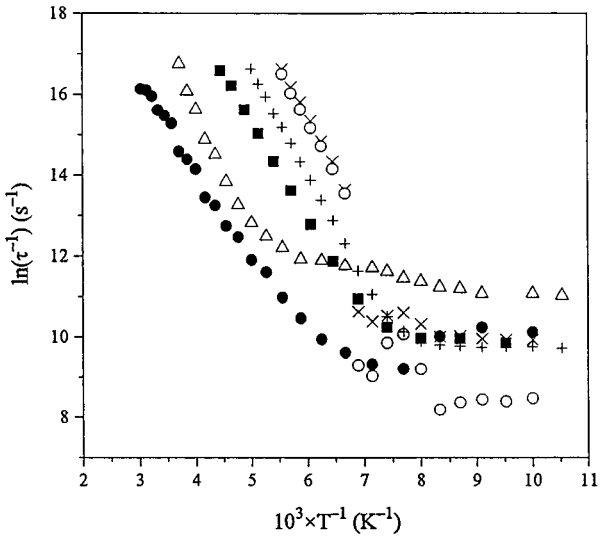

Figure 4. Plots of ln(τ^{-1}) vus T^{-1} for Pt(II) complexes in 4:1 (v/v) C_2H_5OH/CH_3OH: (△) [Pt(bph)(dppm)]; (×) [Pt(2-phpy)(dppm)](PF_6); (+) [Pt(2-ptpy)(dppm)](PF_6); (■) [Pt(2-phq)(dppm)](PF_6); (○) [Pt(7,8-bzq)(dppm)](PF_6); (●) [Pt(bpy)(dppm)](PF_6)$_2$.

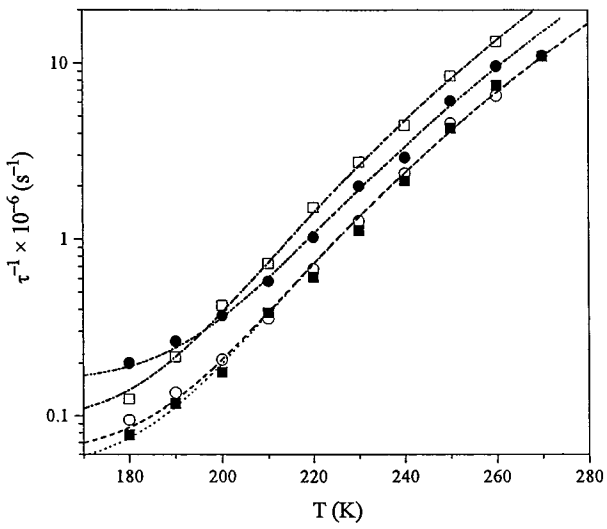

Figure 5. Plots of τ^{-1} vus T for [Pt(bph)(dppm)]: (o) in toluene; (●) in 4:1 (v/v) C_2H_5OH/CH_3OH; (○) in CH_2Cl_2; (■) in *n*-butyronitrile.

Table 7. Parameters for Pt(bph)(dppm) in Different Solvents[a]

solvent	$k_0 \times 10^4$ (s^{-1})	$k_1 \times 10^{12}$ (s^{-1})
n-C_4H_9CN	5.1 ± 1.0	2.3 ± 0.1
CH_2Cl_2	6.2 ± 1.8	2.3 ± 0.04
toluene	9.5 ± 2.1	4.5 ± 0.07
4:1 C_2H_5OH/CH_3OH	16 ± 8	3.1 ± 0.09

[a] E_a was set to be 2300 cm^{-1} for all the three solvents. Errors are from the least-squares fit.

the emission lifetimes decreased rapidly. After the glass-to-fluid transition, changes in emission lifetimes with temperature fell into two categories: for category 1, rapid deactivation of the emitting state continued after the glass-to-fluid transition; for category 2, a slower deactivation initially occurred followed by a rapid deactivation process. All of the complexes fell in the first category except the bph derivative. The activation energies for category 1 complexes were nearly the same (~1800 cm^{-1}). For the bph complex two deactivation processes were observed, one for the glass-to-fluid transition and the other to a higher lying state ~2300 cm^{-1} above the lowest energy emitting state.

Emission quantum yields were measured in 4:1 (v/v) C_2H_5-OH/CH_3OH at 296 K. The quantum yields and the measured or extrapolated lifetimes at 296 K are listed in Table 6. The only compound displaying an appreciable emission lifetime at room temperature was [Pt(bpy)(dppm)]$^{2+}$.

Solvent Effects. As shown in Figure 5, the solvent affects the profiles of emission lifetime vs temperature plots for Pt-(bph)(dppm). Generally, emission lifetimes in CH_2Cl_2 and in *n*-butyronitrile were longer than those in 4:1 (v/v) C_2H_5OH/CH_3OH and in toluene. This suggests that electronically excited Pt(bph)(dppm) interacted more strongly with toluene followed by 4:1 (v/v) C_2H_5OH/CH_3OH, then CH_2Cl_2, and finally *n*-butyronitrile.

The parameters listed in Table 7 were determined using eq 2 by nonlinear least-squares fits. Because of the lifetime−temperature dependence similarity from one solvent, the activation energies were fixed at 2300 cm^{-1}, resulting in the tabulated k_0 and k_1 values. The k_0 value differed from solvent to solvent and ranged from 5.1 × 10^4 s^{-1} in *n*-butyronitrile to 1.6 × 10^5 s^{-1} in 4:1 (v/v) C_2H_5OH/CH_3OH.

Discussion

UV−Vis Absorption Spectra. The trend for the MLCT energy maxima of the platinum(II) dppm complexes, bpy > bph > phen > 2-phpy > 2-ptpy > 2-phq > 7,8-bzq, indicates that the process is a function of the aromatic ligand, its symmetry, degree of aromaticity, and attached electron donor/acceptor groups. The highest energy MLCT transitions occur in the symmetrical bpy and bph complexes. The next highest energy transition takes place in the symmetrical phen complex, which has a greater degree of aromatic character than bpy. The less symmetrical ligand complexes containing the C^N linkage undergo their MLCT transitions at lower energy. In agreement with the bpy−phen comparison above, the complex containing the less aromatic ligand (2-phpy) absorbs at higher energy than those containing the quinoline moiety.

In terms of electron density arguments, the stronger electron-donating ligands tend to localize their electron densities on the metal center, raising the energy of the highest occupied d orbital, while the better π^*-accepting ligands tend to delocalize the electron density from the metal onto itself, lowering the energy

Table 8. Singlet−Triplet Splitting for Pt(II) Complexes (±0.05)

complex	E^1_{MLCT} (10^3 cm^{-1})	$E^3_{LC,}{}^3_{MLCT}$ (10^3 cm^{-1})	ΔE (10^3 cm^{-1})
[Pt(bph)(dppm)]	29.50	19.65	9.85
[Pt(2-ptpy)(dppm)]$^+$	25.97	20.62	5.35
[Pt(2-phpy)(dppm)]$^+$	26.53	20.98	5.55
[Pt(7,8-bzq)(dppm)]$^+$	25.00	21.28	3.72
[Pt(2-phq)(dppm)]$^+$	24.21	19.01	5.20
[Pt(bpy)(dppm)]$^{2+}$	30.03	21.99	8.04
[Pt(phen)(dppm)]$^{2+}$	28.01	22.17	5.84

of the unoccupied π^* energy level. For example, when the chromophoric ligand changed from 2-phpy to 2-ptpy, the electron donation ability of 2-ptpy increases because of the presence of the electron-donating CH_3 group, which increases the electron density on the metal center, making the metal more oxidizable. Therefore, a red spectral absorption shift is expected and observed. For complexes containing 2-phpy and 7,8-bzq (or bpy and phen), the donor atoms are the same, but there is more extensive aromaticity in the 7,8-bzq ligand, which lowers the π^* energy level, causing a red spectral absorption shift as observed. The blue spectral absorption shift of the complex containing bpy compared to the complex containing 2-phpy can be attributed to the decrease in the electron donor ability of the coordinating N^N′ atoms compared to C^N, which lowers the energy of the highest occupied d orbital. In like manner, one might expect the absorption of the [Pt(bph)(dppm)] complex to be blue-shifted from [Pt(bpy)(dppm)]$^{2+}$, since C^C′ would be a better electron donor system than N^N′. Apparently, back electron donation into the π^* energy level offsets the greater σ donor ability of the bph ligand, resulting in the observed anomaly.

Emission Properties. Emission energy maxima followed the trend phen > bpy > 7,8-bzq > 2-phpy > 2-ptpy > bph > 2-phq, indicating that emission occurred in the energy order N^N′ donors > C^N donors > C^C′ donors. This trend follows the electron-donating abilities of the coordinating ligands. In the case where the ligands were more rigid (e.g., phen and 7,8-bzq), emission from the complexes occurred at higher energies than their less rigid analogues bpy and 2-phpy.

The energy change between absorption and emission can be quantified by the singlet−triplet splitting, the difference in energy between the absorption and emission energy maxima (Table 8). The splittings fall in the order bph > bpy > phen > 2-phpy > 2-ptpy > 2-phq > 7,8-bzq. The excited-state singlet−triplet splitting is related to the degree of overlap between the molecular orbitals of the electron-accepting state and the orbitals of the emitting state. The more symmetrical complexes containing N^N′ and C^C′ donors give rise to greater splittings than the less symmetrical orthometalled complexes.

The energy level diagram in Figure 6 summarizes the singlet−triplet splitting data. In organic systems, the energy difference, $E_S - E_T$, has large values on the order of 10 000 cm^{-1} for (π,π^*) states and values of about 4000 cm^{-1} for charge-transfer states.[62] If this same analogy holds for the complexes studied here, then the charge-transfer characteristics of the complexes increase as the singlet−triplet splitting decreases.

Emission Lifetimes. Emission lifetimes at 77 K follow the trend phen > 7,8-bzq > 2-ptpy > 2-phq > 2-phpy > bpy > bph. With the exception of the phen derivative, the emission lifetimes correlate inversely with the singlet−triplet splitting. The greater the degree of charge-transfer character, the longer the emission lifetime of the complex at 77 K. The ordering, with the exception of bpy, is N^N′ donors > C^N donors > C^C′ donors, but the ordering within the series is a departure

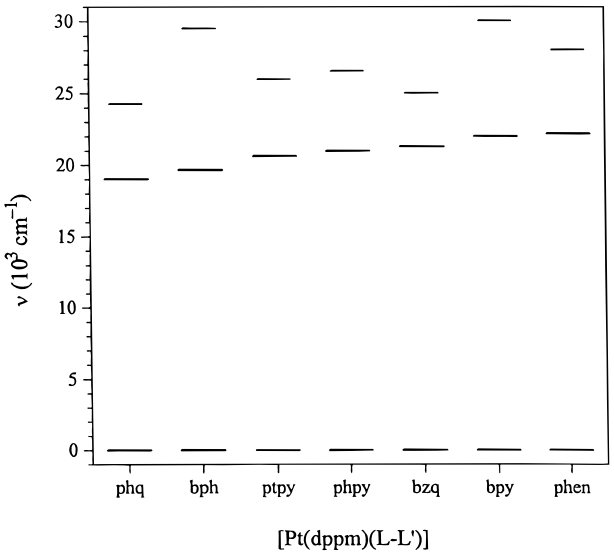

Figure 6. Relative ordering of energy states for Pt(II) complexes. From bottom up are the ground state, the emitting triplet state, and the first singlet excited state.

from the energy gap law based on emission energy maxima. Two possible explanations for this can be given. First, in previous cases where trends followed the energy gap law, the heterocyclic ligand remained the same and either the solvent was varied or the ligands with various substituents were varied. Attempts to make correlations with two different ligand systems failed. The second possible explanation involves variations in the intersystem crossing quantum yields. Previous reports for these complexes indicate that in fluid solution, direct population of the triplet excited state from the ground state enhances the emission process of these complexes, but the enhancement varied from complex to complex.[63]

In fluid solution, the emission lifetimes of the symmetrical N^N′ and C^C′ complexes are the longest despite similar activation energies. In this case, the emission lifetimes of the complexes extrapolated to room temperature nearly paralleled the singlet−triplet splitting. The solvent clearly interacts more strongly with the excited states displaying more charge-transfer character than with those displaying less.

The emission decayed monoexponentially. The slope from a $\ln \tau^{-1}$ vs T^{-1} plot yielded thermal activation to a pathway responsible for additional deactivation of the excited state. The activation energies were similar in all cases and suggest a similar energy barrier leading to an additional nonradiative decay pathway. This supports the argument that the nonradiative decay pathway results from collision of the solvent molecules with the complexes.

Effects of Solvent. The effects of different solvents on the emission lifetimes of Pt(bph)(dppm) were relatively minor. The emission lifetimes in toluene and in 4:1 (v/v) C_2H_5OH:CH_3OH were shorter at temperatures above 200 K than in CH_2Cl_2 and in *n*-butyronitrile. Greater solvent interaction has the effect of facilitating nonradiative decay to the ground state. The enhanced decay in toluene can be attributed to interaction of its π system with that of the bph ligand; in 4:1 (v/v) C_2H_5OH/CH_3OH, the shorter lifetime can be related to hydrogen bonding of the solvent. The fact that the emission lifetime in *n*-butyronitrile is approximately the same as in CH_2Cl_2 would indicate that the open coordination sites of the square planar platinum complex are not strongly coupled to the decay process, since one would

expect *n*-butyronitrile to coordinate with Pt(II) through the cyano group if this were important to excited-state decay.

Conclusions

The photophysical properties of Pt(II) complexes can be modified by changing either the chromophoric ligands or the nonchromophoric ligands. The focus of attention in this report has been on the chromophoric ligand. The emission lifetimes of the complexes depend on the singlet−triplet splitting. As the singlet−triplet splitting decreases, the charge-transfer character of the excited states increases. The result is an increase in emission lifetime at 77 K in a glassy environment, but in solution, the solvent interacts more strongly with excited states displaying charge-transfer character, resulting in diminished emission character. Knowledge of the singlet−triplet splitting as well as the energy gap, the activation energy, the preexponential factor, and the intersystem quantum yield populating the emitting state provides insight into the excited-state deactivation process in emitting transition metal complexes.

Acknowledgment. The authors thank the Office of Basic Energy Sciences of the United States Department of Energy for support, the National Science Foundation for the laser equipment, and Johnson Matthey for the platinum source compound on loan.

Supporting Information Available: Tables listing additional data collection and refinement parameters, atomic coordinates, anisotropic displacement parameters, bond lengths and angles involving nonhydrogen atoms for **1** (Tables S1 − S5), **2** (Tables S6−S10), **3** (Tables S11−S15), and **4** (Tables S16−S20) and drawings of **1**−**4**. This material is available free of charge via the Internet at http://pubs.acs.org.

IC991306D